On Plasma Start-Up in the FREED Device

F. L. M. Müller, M. Martin, M. L. Enghofer, H. He, A. Marinoni, S. I. Krasheninnikov

February 2026

Abstract

We assess the possibility of plasma initiation in the FREED device by the electric breakdown of the gas filling the chamber in the vicinity of the X-point with an inductive electric field. We perform numerical simulations of the electron dynamics in the vacuum magnetic and inductive electric fields. Different settings of the coils producing a vacuum magnetic field were considered. The goal is to achieve an avalanche breakdown, leading to an exponential increase in the electron population around the X-point. Both the 2:1 and 1:2 configurations achieve successful breakdown at $\varepsilon \geq 4 \times 10^{-7}$ (703V loop voltage), with the 2:1 configuration exhibiting 41% higher growth rate scaling.

1 Motivation

The simplicity of the magnetic plasma confinement in a dipolar configuration makes such plasma quite attractive for the application to magnetic fusion [1–5]. However, it has a significant downside—the necessity to levitate the coil producing the dipolar magnetic field to avoid plasma-material interactions. Whereas such a drawback of the dipolar plasma confinement is manageable for small-scale experiments, it can result in a severe issue for a large-scale fusion reactor.

Recently [6], a novel dipole-like symmetric magnetic configuration suitable for a fusion plasma confinement was suggested. In this configuration, the dipolar-like magnetic field is formed by the combination of the magnetic field provided by structurally supported current-carrying coils and the plasma diamagnetic current. As a result, a separatrix disconnects the plasma-occupied magnetic flux surfaces from the rest of the magnetic field lines. Therefore, plasma is "free" and not wrapped around any coil as it does in the original dipolar configuration [1–5].

In this work, we assess the possibility of plasma initiation in the FREED device by the electric breakdown of the gas, filling the chamber, in the vicinity of the X-point with an inductive electric field.

2 Equations and Parameters

In the actual simulation, only dimensionless equations and parameters were used to ensure comparability and to provide a timescale suitable for capturing the cyclotron motion of the singular electrons moving in the magnetic field.

For this we define a "reference" magnetic field and spatial scale: $R^* = 1$ m, $B^* = 1$ kGauss, $V_{ion} \sim 3{\cdot}10^8$ cm/s. Together with the speed of light c, the elemental charge e of an electron and its mass m_e this allows us to fully define the governing equations. The parameters used are:

$$\hat{r} = \frac{r}{R_*}, \quad \hat{t} = t\Omega_*, \quad \hat{V} = \frac{V}{V_*}, \quad W_{ion} = \frac{V_{ion}}{V_*} \tag{1}$$

$$\Omega_* = \frac{|e|B_*}{m_e c}, \quad V_* = R_*\Omega_* \tag{2}$$

Resulting in the dimensionless electric field $\varepsilon = c\frac{E}{B_* V_*}$ ($|\varepsilon| \ll 1$), as well as the dimensionless fluxes:

$$\hat{\Psi}_B = \frac{\Psi_B}{R_*^2 B_*} \quad \text{and} \quad \Psi_E = \varepsilon B_* R_* V_* \tag{3}$$

Here $\hat{\psi}_B$ describes the dimensionless magnetic flux due to infinitely thin toroidal coils:

$$\hat{\psi}_B(\hat{R}, \hat{z}) = \sum_i \frac{\hat{I}_i}{2\hat{R}_i}\, \hat{R}\, G(\kappa_i) \tag{4}$$

where $\hat{I}_i = \frac{4I_i}{cR_*B_*}$, $G(\kappa) = \frac{(2-\kappa^2)K(\kappa^2) - 2E(\kappa^2)}{\kappa}$, $\kappa_i^2 = \frac{4\hat{R}_i\hat{R}}{\hat{R}_i^2 + 2\hat{R}_i\hat{R} + \hat{R}^2 + (\hat{z}-\hat{z}_i)^2}$, and K, E are the complete elliptic integrals of the First and Second Kind respectively.

2.1 Equations of Motion

There are three directions of interest, $\hat{V}_R$, $\hat{V}_z$ and the velocity in toroidal direction $\hat{V}_\varphi$. We need to calculate $\hat{V}_\varphi$ from the position and time passed:

$$\hat{V}_\varphi = \frac{1}{\hat{R}}\Big(\varepsilon\hat{t} + \hat{\Psi}_B(\hat{R}, \hat{z}) - \hat{\Psi}_B(\hat{R}_0, \hat{z}_0)\Big) \tag{5}$$

Velocity in R and z are obtained using a numerical method for solving ODEs and are governed by:

$$\frac{d\hat{V}_R}{d\hat{t}} = \frac{\hat{V}_\varphi}{\hat{R}}\left(\hat{V}_\varphi - \frac{\partial\hat{\Psi}_B}{\partial\hat{R}}\right), \quad \frac{d\hat{V}_z}{d\hat{t}} = -\frac{\hat{V}_\varphi}{\hat{R}}\frac{\partial\hat{\Psi}_B}{\partial\hat{z}} \tag{6}$$

While the position is obtained by integrating the velocity:

$$\frac{d\hat{R}}{d\hat{t}} = \hat{V}_R, \quad \frac{d\hat{z}}{d\hat{t}} = \hat{V}_z \tag{7}$$

2.2 Ionization Criteria

The traditional ionization criterion of 10eV corresponds to a velocity of $V_{ion} \sim 3 \cdot 10^8$ cm/s. However, the nature of the non-dimensionalization puts us in the unique position, that if we lower the ionization threshold from what was initially $\hat{T}_1 = 1.45 \times 10^{-8}$ to a value lower than that, $\hat{T}_2 = \hat{T}_1/3$, this then corresponds to a dimensional kinetic energy of 10eV, if the problem had been normalized with a weaker reference magnetic field B^*:

$$\hat{T}_{ion} = \frac{T_{ion}}{m_e V_*^2} \propto \frac{1}{B_*^2} \quad \Rightarrow \quad \frac{\hat{T}_{ion,2}}{\hat{T}_{ion,1}} = \frac{1}{3} \Leftrightarrow B_{*,2} = \frac{B_{*,1}}{\sqrt{3}} \tag{8}$$

In the following the "higher" ionization threshold will be referred to as criterion **1** and the "lower" motivated by correspondence to the weaker magnetic field will be called criterion **2**.

3 Characteristics of the FRED

FRED standing for **F**ast **R**eliable **E**lectron **D**ynamics is the tool written in C, that was developed in order to simulate the electron dynamics inside the different coil configurations in the presence of different electric field strengths. It uses the GNU-scientific library for elliptic integrals and 2D-bicubic interpolation to 3rd order accuracy.

The tool only considers collisionless electron dynamics in the presence of a perfectly symmetric toroidal electric field and a magnetic field defined by infinitely thin coils. We try to find conditions necessary to achieve an electron kinetic energy E_{kin} exceeding the previously discussed criteria.

After this energy is reached, two new electrons are launched, starting at the last position of the previous electron with $0.5 \cdot E_{kin}$ and a random velocity direction. These new electrons are added into a queue that is ordered in ascending order by the global initial time of each electron, ensuring accurate unraveling of the lineage tree into a one-dimensional array. Electrons that leave the vicinity of the X-point do not spawn any offspring and are assumed to have escaped. The current state of the electrons, $(\hat{V}_r, \hat{V}_z, \hat{R}, \hat{z})$, is calculated using the RK4 integration scheme with a fixed time step size of $d\hat{t} = 0.1$.

4 Results

Two three-coil configurations were studied. A distinction is made between having one or two coils on the outside.

2:1 Configuration: Two coils are placed at a shorter radius than one coil which is placed at a radius further out. Parameters: $[(\hat{R}_i, \hat{z}_i, \hat{I}_i)] = [(1, -0.5, 1); (1, 0.5, 1); (2, 0, 0.144)]$, giving an X-point at about $(\hat{R}, \hat{z}) = (1.48628, 0)$.

1:2 Configuration: One coil on the inside and two coils on the outside. Parameters: $[(1, 0, 1); (2, 0.5, 0.151); (2, -0.5, 0.151)]$, giving an X-point at about $(1.8087, 0)$.

4.1 Minimum Breakdown Threshold

Both configurations achieve avalanche breakdown at minimum $\varepsilon = 4 \times 10^{-7}$ (703V loop voltage) for criterion **1**. Field strengths below this value were not able to provide any kind of sustained growth and showed a continuous decline in population after an initial peak. This is a strong indication that the electrons were not able to reach the ionization energy before escaping, leading to a population die-out.

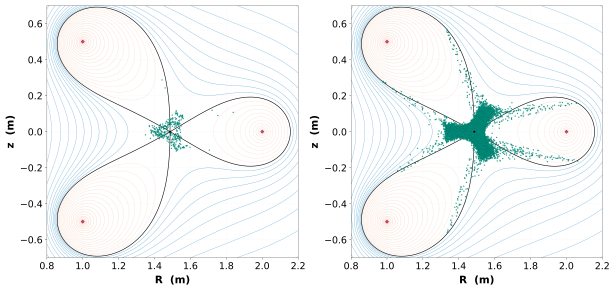

Figure 1: Electron evolution for $V_{loop} = 703$V, showing avalanche breakdown at discrete time snapshots.

More information about the desired breakdown can be obtained by plotting the position of all individual electrons present in the reactor at discrete instances of time, as shown in Fig. 1. Field strengths high enough show steep increases in the number of electrons in the vicinity of the X-point. Here we can also observe, that the most common avenue of escape is along the isolines of the separatrix. Secondly escape outwards was more common than escape inwards, a phenomenon that can be attributed to the centrifugal force aiding escape outwards and disadvantaging escape inwards.

Clearly the field strength $\varepsilon = 4 \times 10^{-7}$, corresponding to a loop voltage of 703V, is able to show exponential growth. The equation of the fitted exponential is:

$$N(t) = 31.167 \cdot e^{0.0003t} \tag{9}$$

where $\hat{t}$ can be converted to a doubling time of $t_d = \frac{\ln(2)}{0.0003} \approx 2310$ in dimensionless units, corresponding to about 131.5 ns in SI units.

For criterion **2** the boundary found is 62.5% lower at $\varepsilon = 1.5 \times 10^{-7}$ (263.7V loop voltage), demonstrating that lowering the ionization threshold significantly reduces the minimum required field strength.

4.2 Linear Growth Rate Scaling

Establishing that different field strengths show different growth rates, we now compare the growth rates

of different epsilon values. For this the same process was repeated for a number of different epsilon values, greater than 4×10^{-7}, producing a plot of the exponential growth rates over the field strength ε, depicted in Fig. 2.

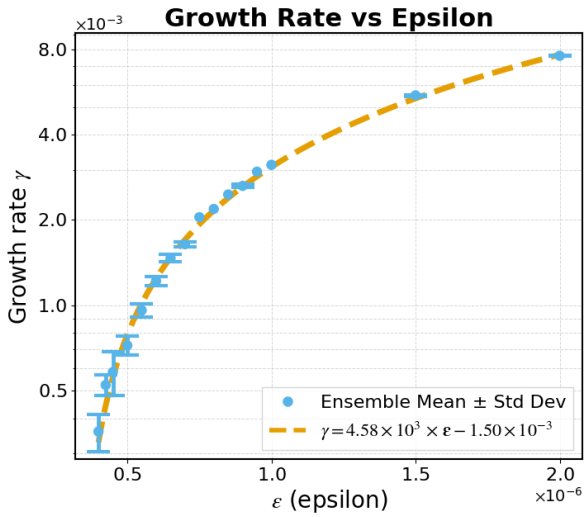

Figure 2: Growth rate of the exponential fit over the field strength ε for the 2:1 configuration.

Examination of Fig. 2 shows a clear linear trend in the exponential growth factor over increasing field strength ε. The linear regression lines are given by the following equations:

2:1 Configuration (Criterion 1):

$$\gamma(\varepsilon) = 4.58 \times 10^3 \varepsilon - 1.5 \times 10^{-3} \tag{10}$$

1:2 Configuration (Criterion 1):

$$\gamma(\varepsilon) = 3.24 \times 10^3 \varepsilon - 6.64 \times 10^{-4} \tag{11}$$

2:1 Configuration (Criterion 2):

$$\gamma(\varepsilon) = 7.33 \times 10^3 \varepsilon - 9.71 \times 10^{-4} \tag{12}$$

This increase essentially consists of two, related, effects. First the higher field strengths allow for faster acceleration, naturally leading to a stronger growth over time. Secondly, we see a decrease in spread of the electrons, that might be explained by the fact that fast acceleration prevents a strong migration before the ionization energy is reached, at which two new random directions are assigned.

4.3 Physical Interpretation

We can observe a linear dependence for every configuration and ionization criteria tested. In the following will be an argument as to why that should be the case.
By definition of the non-dimensional field strength the energy gained per cyclotron orbit is linearly dependent on ε:

$$\Delta \hat{E}_{orbit} = \oint q\mathbf{E} \cdot d\mathbf{l} \propto \varepsilon \tag{13}$$

The time it then takes to accelerate up to the ionization boundary is inversely dependent on the energy gained per orbit as the orbit frequency itself is constant due to the character of our non dimensionalization in the vicinity of the X-point:

$$\hat{t}_{ion} \propto \frac{\hat{T}_{ion}}{\Delta \hat{E}_{orbit} \cdot f_{orbit}} \propto \frac{1}{\varepsilon} \tag{14}$$

And then lastly we see that a lower $\hat{t}_{ion}$ results in a lower $\hat{t}_d$ and γ on the other hand inversely depends on the doubling times:

$$\hat{t}_d = \frac{\ln 2}{\gamma} \propto \frac{1}{\varepsilon} \quad \Rightarrow \quad \gamma \propto \varepsilon \tag{15}$$

This gives us the following ideal expression for gamma with all electrons staying in the vicinity of the X-point:

$$\gamma_{ideal} = \frac{\ln 2 \cdot \Delta \hat{E}_{orbit} \cdot f_{orbit}}{\hat{T}_{ion}} \propto \varepsilon \tag{16}$$

Reverting our focus to the linear behaviour at hand we see that the relationship exhibits a slope smaller than the idealized version. This is partially due to the previously stated behaviour of electrons escaping the X-point vicinity. Considering all these different nuances we expect a linear behaviour with a slope smaller than the idealized behaviour previously discussed:

$$\gamma(\varepsilon) = \underbrace{4.58 \times 10^3}_{\text{field-driven growth}} \cdot \varepsilon \underbrace{-1.5 \times 10^{-3}}_{\text{constant loss}} \tag{17}$$

4.4 Comparison of Configurations

Having justified the linearity of the relation between the exponential growth factor and ε via Eqs. (13)–(16), we also recognize that while both exhibit the same threshold, they do differ in the equation of the actual fit given by Eqs. (10) and (11). This results in a ratio of the slopes:

$$\frac{\gamma_{2:1}}{\gamma_{1:2}} = \frac{4.58 \times 10^3}{3.24 \times 10^3} \approx 1.41 \tag{18}$$

This difference in slopes has to directly arise from the difference in geometry of the nested flux surfaces produced by the inversion of the coil placements as all other parameters were kept the same across both simulations. The X-point resides about 0.32 further inward in dimensionless units for the 2:1 configuration. This combination of X-point position and forced diagonal escape trajectory leads to a higher average success rate for the same non dimensional field strength and thus to a higher slope in the linear fit as expressed in Eq. (10).

5 Validation

As the off-springs of each electron are given a random initial velocity direction we cannot directly reproduce the results. However, the population growth is averaged across multiple simulations with the same initial conditions, allowing for a more robust comparison. We clearly observed a consistent decrease of magnitude in standard deviation for an increasing number of simulations.
Energy conservation validation shows normalized errors $\sim 10^{-12}$ (six orders below initial electron energy), with no visible correlation between ionization events and spikes in error. Non-normalized errors remain $\sim 10^{-4}$, confirming numerical accuracy is preserved across energy handoff at offspring generation.

6 Conclusion

The goal of this work was to investigate the possibility of plasma start-up in the FREED device by the electric breakdown of the gas, filling the chamber, in the vicinity of the X-point with an inductive electric field.
The results show that the 2:1 as well as the 1:2 configuration were both able to produce a successful avalanche at comparable field strengths, with minimum threshold $\varepsilon = 4 \times 10^{-7}$ (703V) achieving sub-microsecond breakdown timescales. The 2:1 configuration demonstrates 41% higher growth rate scaling via geometric confinement advantages as shown in Eq. (18).
While we are confident in the results obtained, we also acknowledge the limitations and omissions of the tool, such as electron-electron interactions, perfect toroidal symmetry, the assumption of infinitely thin coils, as well as actual collisions with the background gas.

References

[1] A. Hasegawa, Comments Plasma Phys. Control. Fusion **11** (1987) 147.

[2] S. I. Krasheninnikov et al., Phys. Rev. Lett. **82** (1999) 2689.

[3] D. T. Garnier et al., Phys. Plasmas **13** (2006) 056111.

[4] J. Kesner et al., Plasma Phys. Control. Fusion **52** (2010) 124036.

[5] M. S. Davis et al., Plasma Phys. Control. Fusion **56** (2014) 095021.

[6] S. I. Krasheninnikov et al., Phys. Plasmas **32** (2025) 114501.